Enhancement of Permanent Magnet Synchronous Machines Torque Estimation Using Pulsating High Frequency Current Injection

Maria Martinez, David Reigosa, Daniel Fernández, J. M. Guerrero and Fernando Briz
*University of Oviedo. Dept. of Elect., Computer & System Engineering, Gijón, 33204, Spain.
martinezgmaria@uniovi.es, diazdavid@uniovi.es, fernandezalodaniel@uniovi.es, guerrero@uniovi.es, fernando@isa.uniovi.es

Abstract: Torque estimation in permanent magnet synchronous machines is highly desirable in many applications. Torque produced by a permanent magnet synchronous machine depends on the permanent magnets' flux and *dq*-axes inductances. Consequently, precise knowledge of these parameters is required for proper torque estimation. This paper proposes the use of a high frequency signal for both PM flux and *dq*-axes inductances estimation. The high frequency signals will be injected in the stator via inverter superposed on top of the fundamental excitation. The proposed method can be used without interfering with the normal operation of the machine, the results being highly insensitive from machine's working condition.[1]

***Index Terms* — High frequency signal injection, permanent magnet synchronous machines, online parameters estimation, torque estimation.**

I. Introduction

Design and control of permanent magnet synchronous machines (PMSMs) have been the focus of significant research efforts during the last decades due to their high dynamic performance, torque density and efficiency. Many applications require precise control of the torque produced by the machine, torque measurement/estimation being therefore a highly interesting feature.

If torque is to be measured, torque transducers based on strain gauges are likely the preferred option [1]-[5]. However, this type of sensors can introduce resonances into the system, are highly sensitive to electromagnetic interference and their cost could account for a significant portion of the drive cost [6]. Less popular alternatives for torque measurement are systems based on torsional displacement [7]. Torsional displacement methods are immune to electromagnetic noise but they use optical probes, which are expensive and require accurate calibration [7]. Regardless of the method being used, precise torque measurement is expensive, requires room and extra cables, torque estimation being therefore preferred.

Torque estimation methods can be roughly classified into those based on the torque equation [8]-[9] and indirect estimation methods [10]-[18]. Torque equation methods include methods based on general torque equation [8], flux estimation [8] or look-up-tables [9]. Indirect estimation methods include methods based on the electric power and rotor speed [10], observer based methods [11]-[16] (e.g. sliding mode observers [11], model reference adaptive systems [12]-[13], model reference observers, reduced order observers [14], recursive least square parameters estimation [15] or affine projection algorithms parameters estimation [16]), methods requiring additional sensors, e.g. giant magnetoresistance effect (GMR) based methods [17], or neural networks based methods [18]. All these methods [8]-[18] require previous knowledge of certain machine parameters and/or its operating condition (e.g. temperature, resistances or inductances).

It is known that PM remanent flux and *dq*-axes inductances change during the normal operation of the machine due to fundamental current injection [19]-[20] and PM temperature [19]-[21]. An increase of the PM temperature reduces the PM remanent flux (i.e. magnetization state) reducing therefore the machine torque for a given stator current. In addition PM remanent flux variation changes the *d*-axis saturation level (assumed that the PMs are aligned with the *d*-axis), making the *d*-axis inductance to change [22]. Injection of fundamental *dq*-axes current changes the *dq*-axes saturation level, resulting therefore in *dq*-axes inductances variation [22], [23]. Therefore, to obtain reliable torque estimation, knowledge of parameters variation with machine operating conditions would be required.

In this paper, online torque estimation for PMSMs combined with parameter identification is proposed. Machine parameters are estimated from the response to two HF signals injected in the stator terminals of the machine via inverter. The HF signals are superposed on top of the fundamental excitation, meaning that the method will not interfere with the normal operation of the machine, the results being highly insensitive from machine's working conditions (i.e. saturation and temperature effects).

The paper is organized as follows: fundamental model of a PMSM is presented in section II. Parameter identification and

[1] This work was supported in part by the Research, Technological Development and Innovation Programs of the Spanish Ministry Economy and Competitiveness, under grant MINECO-17-ENE2016-80047-R and by the Government of Asturias under project IDI/2018/000188 and FEDER funds.

torque estimation in PMSMs using a HF signal is presented in section III, whereas implementation of the method and experimental results are provided in section IV. Finally, conclusions are presented in section V.

II. Fundamental model of a PMSM

The fundamental model of a PMSM in a reference frame synchronous with the rotor is given by (1), [19], where R_d, R_q, L_d and L_q are the d and q-axis resistances and inductances respectively and λ_{pm} is the PM flux. The output torque can be expressed by (2), where P is the number of poles [19]. The first term on the left-hand side of (2), T_{syn}, is the electromagnetic/synchronous torque, while the second term on the right-hand side of (2), T_{rel}, is the reluctance torque. It can be concluded from (2) that T_{syn} estimation requires λ_{pm} estimation, while T_{rel} requires differential inductance, i.e. L_d-L_q, estimation. It will be shown in the next section that λ_{pm}, L_d and L_q can be estimated by injecting two high frequency (HF) signals into the stator terminals of a PMSM. In the nomenclature used it this paper, superscripts "s" and "r" indicate the stationary and rotor synchronous reference frames respectively; subscripts "s" and "r" indicate stator and rotor variables, while subscripts "dq" and "HF" indicate fundamental and HF components respectively. Finally, * is used to indicate commanded values while ^ indicates estimated values.

$$\begin{bmatrix} v_{sd}^r \\ v_{sq}^r \end{bmatrix} = \begin{bmatrix} R_d & 0 \\ 0 & R_q \end{bmatrix} \begin{bmatrix} i_{sd}^r \\ i_{sq}^r \end{bmatrix} + p \begin{bmatrix} L_d & 0 \\ 0 & L_q \end{bmatrix} \begin{bmatrix} i_{sd}^r \\ i_{sq}^r \end{bmatrix} + \begin{bmatrix} 0 & -\omega_r L_q \\ \omega_r L_d & 0 \end{bmatrix} \begin{bmatrix} i_{sd}^r \\ i_{sq}^r \end{bmatrix} + \begin{bmatrix} 0 \\ \lambda_{pm}\omega_r \end{bmatrix} \quad (1)$$

$$T_{out} = \frac{3}{2}\frac{P}{2}\left[\lambda_{pm} i_{sq}^r + \left(L_d - L_q\right) i_{sd}^r i_{sq}^r\right] = T_{syn} + T_{rel} \quad (2)$$

III. Parameter identification and torque estimation in PMSMs using a HF signal

This section analyzes the physical principles of torque estimation in PMSMs using HF signal injection.

A) HF model of a PMSM

If the PMSM is fed with a HF voltage/current, the magnet flux dependent term in (1) can be safely neglected, as it does not contain any HF component, the resulting HF model being (3) [23].

$$\begin{bmatrix} v_{sdHF}^r \\ v_{sqHF}^r \end{bmatrix} = \begin{bmatrix} R_{dHF} & 0 \\ 0 & R_{qHF} \end{bmatrix} \begin{bmatrix} i_{sdHF}^r \\ i_{sqHF}^r \end{bmatrix} + p \begin{bmatrix} L_{dHF} & 0 \\ 0 & L_{qHF} \end{bmatrix} \begin{bmatrix} i_{sdHF}^r \\ i_{sqHF}^r \end{bmatrix} + \begin{bmatrix} 0 & -\omega_r L_{qHF} \\ \omega_r L_{dHF} & 0 \end{bmatrix} \begin{bmatrix} i_{sdHF}^r \\ i_{sqHF}^r \end{bmatrix} \quad (3)$$

If the frequency of the injected HF signal is sufficiently higher than the rotor frequency, the rotor speed dependent terms can also be safely neglected, the simplified HF model shown in (4) being obtained. An indicative threshold for this assumption can be $\omega_{hf} > \omega_r + 2\cdot\pi\cdot 500$ [23].

$$\begin{bmatrix} v_{sdHF}^r \\ v_{sqHF}^r \end{bmatrix} = \begin{bmatrix} R_{dHF} & 0 \\ 0 & R_{qHF} \end{bmatrix} \begin{bmatrix} i_{sdHF}^r \\ i_{sqHF}^r \end{bmatrix} + p \begin{bmatrix} L_{dHF} & 0 \\ 0 & L_{qHF} \end{bmatrix} \begin{bmatrix} i_{sdHF}^r \\ i_{sqHF}^r \end{bmatrix} \quad (4)$$

B) D-axis inductance identification and electromagnetic torque estimation

As shown in (2), electromagnetic torque (T_{syn}) estimation requires knowledge of PM flux, λ_{pm}. D-axis inductance can be used for this purpose as it has been shown to vary almost linearly with PM flux [23], [25]. λ_{pm} variation with d-axis inductance can be expressed as (5).

$$\lambda_{pm} = \left(\lambda_{pm0} + k_{dPM}\frac{L_{d(Id,Iq,T_r)} - L_{d0}}{L_{d0}}\right) \quad (5)$$

where λ_{pm0} and L_{d0} are the PM flux and d-axis inductance at the room temperature (T_{r0}) and when there is no dq-axes fundamental current, $L_{d(Id.Iq,Tr)}$ is the d-axis inductance when the magnet temperature is T_r and there is dq-axes current, and k_{dPM} is the coefficient linking the d-axis inductance and the PM flux.

D-axis inductance (6) is a function of the fundamental current, d and q-axis currents, and PMs remanent flux, which varies with its temperature T_r [22].

$$L_{d(Id,Iq,T_r)} = L_{d0}\left(1 + \alpha_{Id} I_{sd}^r + \alpha_{Iq} I_{sq}^r + \alpha_{T_r}\left(T_r - T_{r0}\right)\right) \quad (6)$$

where α_{Id}, α_{Iq}, α_{Tr} are the coefficients linking the d-axis inductance with the d-axis fundamental current (I_{sd}^r), q-axis fundamental current (I_{sq}^r) due to cross-coupling and magnet temperature (T_r) respectively. D-axis inductance varies with I_{sd}^r and with PM remanent flux due to saturation, the remanent flux being affected by magnet temperature [19], [23]. Equation (6) evidences the difficulties of modeling the behavior of the d-axis inductance, L_d, its estimation from the d-axis HF inductance is discussed following.

D-axis HF inductance can be obtained by injecting a pulsating d-axis HF current (7) into the stator terminals of the machine. A resonant controller can be used for this purpose [23]. The HF voltages commanded by the resonant controller are of the form shown in (8), from which a fictitious HF voltage vector consisting only of the d-axis component $v_{sdqHF1}^{r'}$, (9) is obtained. Both (7) and (9) can be separated into positive sequence ($i_{sdqHF1pc}^{r*}$ and $v_{sdqHF1pc}^{r'}$) and negative sequence ($i_{sdqHF1nc}^{r*}$ and $v_{sdqHF1nc}^{r'}$) components, (10) and (11), each magnitude of half of the original signal. The d-axis HF impedance, (12), can be obtained either from the positive or negative sequence components. The d-axis HF inductance is finally obtained as the imaginary part of (12) (13).

$$i^{r^*}_{sdqHF1} = \begin{bmatrix} \bar{I}^{r^*}_{sdHF1} \\ \bar{I}^{r^*}_{sqHF1} \end{bmatrix} = \begin{bmatrix} I^*_{HF}\cos(\omega_{dHF}t) \\ 0 \end{bmatrix} \tag{7}$$

$$v^{r^*}_{sdqHF1} = \begin{bmatrix} \bar{V}^{r^*}_{sdHF1} \\ \bar{V}^{r^*}_{sqHF1} \end{bmatrix} = \begin{bmatrix} (R_{dHF} + j\omega_{dHF}L_{dHF})\bar{I}^{r}_{sdHF1} \\ \omega_r L_{dHF}\bar{I}^{r}_{sdHF1} \end{bmatrix} \tag{8}$$

$$v^{r'}_{sdqHF1} = \begin{bmatrix} \bar{V}^{r^*}_{sdHF1} \\ 0 \end{bmatrix} = \begin{bmatrix} (R_{dHF} + j\omega_{dHF}L_{dHF})\bar{I}^{r}_{sdHF1} \\ 0 \end{bmatrix} = \begin{bmatrix} V^{r'}_{sdqHF1}\cos(\omega_{dHF}t + \varphi_{Zd}) \\ 0 \end{bmatrix} \tag{9}$$

$$i^{r^*}_{sdqHF1} = \frac{I^*_{HF}}{2}e^{j\omega_{dHF}t} + \frac{I^*_{HF}}{2}e^{-j\omega_{dHF}t} = i^{r^*}_{sdqHF1pc} + i^{r^*}_{sdqHF1nc} \tag{10}$$

$$v^{r'}_{sdqHF1} = \frac{\left|v^{r'}_{sdqHF1}\right|}{2}e^{j(\omega_{dHF}t-\varphi_{Zd})} + \frac{\left|v^{r'}_{sdqHF1}\right|}{2}e^{j(-\omega_{dHF}t+\varphi_{Zd})} = v^{r'}_{sdqHF1pc} + v^{r'}_{sdqHF1nc} \tag{11}$$

$$Z_{dHF} = R_{dHF} + j\omega_{dHF}L_{dHF} = \frac{v^{r'}_{sdqHF1pc}}{i^{r^*}_{sdqHF1pc}} = \frac{v^{r'}_{sdqHF1nc}}{i^{r^*}_{sdqHF1nc}} \tag{12}$$

$$L_{dHF} = \frac{\Im[Z_{dHF}]}{j\omega_{dHF}} \tag{13}$$

In general $L_{dHF(Id.Iq,Tr,fhf)}$ is a function of the fundamental current level, magnet temperature and frequency of the HF signal. Fig. 1 shows the measured *d*-axis HF inductance $L_{dHF(Id.Iq,Tr)}$ of the test machine that will be used for the method verification vs. the frequency of the HF signal, for different fundamental current levels and PMs temperatures. For f_{HF}=0Hz, $L_{dHF} = L_d$ holds (of course a DC excitation is not properly a HF excitation). Note also that $L_d = L_{d0}$ when no fundamental current is injected and PMs are at room temperature (see (6)). It is observed from Fig. 1 that the *d*-axis HF inductance decreases almost linearly as the frequency of the HF signal increases, this behavior being modeled as (14). λ_{pm} variation shown in (5) can be therefore rewritten as (15) after substituting (14) into (5). The synchronous torque (16), $T_{syn,}$ is finally obtained combining (15) and (2). The described process is schematically shown in Fig. 2.

$$L_d = k_{f_{dHF}}L_{dHF} \tag{14}$$

$$\lambda_{pm} = \left(\lambda_{pm0} + k_{dPM}\frac{L_{dHF(Id,Iq,T_r)} - L_{dHF_0}}{L_{dHF_0}}\right) \tag{15}$$

$$T_{syn} = \frac{3}{2}\frac{P}{2}\left[\left(\lambda_{pm0} + k_{dPM}\frac{L_{dHF(Id,Iq,T_r)} - L_{dHF_0}}{L_{dHF_0}}\right)i^r_{sq}\right] \tag{16}$$

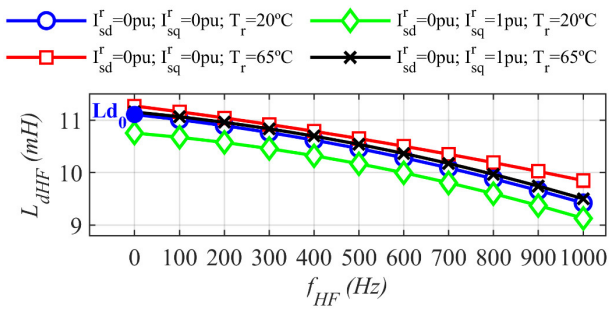

Fig. 1.- *D*-axis HF inductance L_{dHF} variation with f_{HF} for different values of I^r_{sd} , I^r_{sq} and T_r combinations. $\omega_r = 2\cdot\pi$ 50 rad/s.

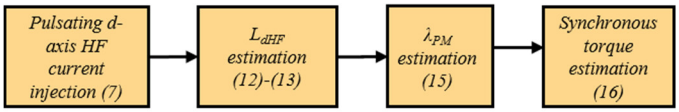

Fig. 2.-. Schematic representation of the process followed to estimate the synchronous torque using pulsating HF current injection.

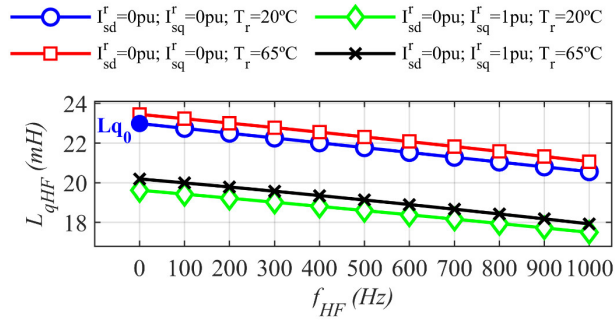

Fig. 3.- *Q*-axis HF inductance L_{qHF} variation with f_{HF} for different values of I^r_{sd} , I^r_{sq} and T_r combinations. $\omega_r = 2\cdot\pi$ 50 rad/s.

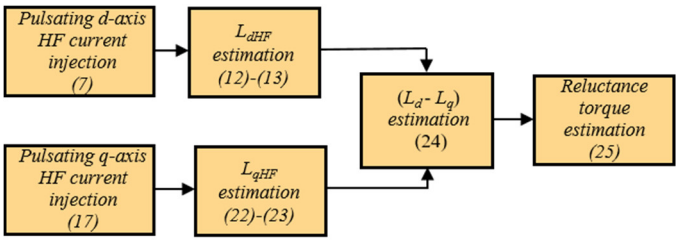

Fig. 4.-. Schematic representation of the process followed to estimate the reluctance torque using pulsating HF current injection.

C) Q-axis inductance identification and reluctance torque estimation

As shown in (2), reluctance torque (T_{rel}) estimation requires knowledge of the differential inductance (L_d - L_q). *D*-axis HF inductance (L_{dHF}) can be estimated as described in the preceding subsection. Q-axis HF inductance (L_{qHF}) can be estimated by injecting a pulsating *q*-axis HF current (17), the equations describing the process (18)-(23) being equivalent to (8)-(13).

$$i^{r^*}_{sdqHF2} = \begin{bmatrix} \bar{I}^{r^*}_{sdHF2} \\ \bar{I}^{r^*}_{sqHF2} \end{bmatrix} = \begin{bmatrix} 0 \\ I^*_{HF}\cos(\omega_{qHF}t) \end{bmatrix} \tag{17}$$

$$v^{r*}_{sdqHF2} = \begin{bmatrix} \bar{V}^{r*}_{sdHF2} \\ \bar{V}^{r*}_{sqHF2} \end{bmatrix} = \begin{bmatrix} \omega_r L_{qHF} \bar{I}^{r}_{sqHF2} \\ \left(R_{qHF} + j\omega_{qHF} L_{qHF}\right) \bar{I}^{r}_{sqHF2} \end{bmatrix} \quad (18)$$

$$v^{r'}_{sdqHF2} = \begin{bmatrix} 0 \\ \bar{V}^{r*}_{sqHF2} \end{bmatrix} = \begin{bmatrix} 0 \\ \left(R_{qHF} + j\omega_{qHF} L_{qHF}\right) \bar{I}^{r}_{sqHF2} \end{bmatrix} = \begin{bmatrix} 0 \\ V^{r'}_{sdqHF2} \cos\left(\omega_{qHF} t + \varphi_{Zq}\right) \end{bmatrix} \quad (19)$$

$$i^{r*}_{sdqHF2} = \frac{I^{*}_{HF}}{2} e^{j\omega_{qHF} t} + \frac{I^{*}_{HF}}{2} e^{-j\omega_{qHF} t} = i^{r*}_{sdqHF2\,pc} + i^{r*}_{sdqHF2\,nc} \quad (20)$$

$$v^{r'}_{sdqHF2} = \frac{\left|v^{r'}_{sdqHF2}\right|}{2} e^{j\left(\omega_{qHF} t - \varphi_{Zq}\right)} + \frac{\left|v^{r'}_{sdqHF2}\right|}{2} e^{j\left(-\omega_{qHF} t + \varphi_{Zq}\right)} = v^{r'}_{sdqHF2\,pc} + v^{r'}_{sdqHF2\,nc} \quad (21)$$

$$Z_{qHF} = R_{qHF} + j\omega_{qHF} L_{qHF} = \frac{v^{r'}_{sdqHF2\,pc}}{i^{r*}_{sdqHF2\,pc}} = \frac{v^{r'}_{sdqHF2\,nc}}{i^{r*}_{sdqHF2\,nc}} \quad (22)$$

$$L_{qHF} = \frac{\Im\left[Z_{qHF}\right]}{j\omega_{qHF}} \quad (23)$$

Fig. 3 shows the q-axis HF inductance L_{qHF}, vs. the frequency of the HF signal for the test machine at different fundamental current levels and PMs temperatures. As for the d-axis inductance, q-axis HF inductance also decreases as the frequency of the HF signal increases; L_d-L_q, see (2), can be therefore expressed as (24), where k_{fqHF} is the coefficient linking L_{qHF} and L_q (i.e. applying (14) to the q-axis); being k_{fqHF} also approximately equal for the different machine's working conditions, as shown Fig. 3. Finally, L_q and T_{rel} can be estimated from (25) by using (12)-(13), (22)-(24). The described procedure is schematically shown in Fig. 4.

$$\left(L_d - L_q\right) = \left(k_{f_{dHF}} L_{dHF} - k_{f_{qHF}} L_{qHF}\right) \quad (24)$$

$$T_{rel} = \frac{3}{2}\frac{P}{2}\left[\left(k_{f_{dHF}} L_{dHF} - k_{f_{qHF}} L_{qHF}\right) i^{r}_{sd} i^{r}_{sq}\right] \quad (25)$$

IV. Implementation and experimental results

A) Implementation and experimental setup

Fig. 5 shows the general block diagram used for the implementation of the proposed method [23]-[22], including inverter control and injection of pulsating HF signals; torque estimation requires the injection of two pulsating HF signals to estimate L_{dHF} and λ_{pm}, and to estimate L_{qHF} respectively. It must be noted that the frequency of the HF signals in a stationary reference frame will be, $\omega_r + \omega_{hf}$, which should be smaller than half of the switching frequency (i.e. Nyquist frequency) as aliasing would occur otherwise [22]-[24]. In addition, use of the method near or above the nominal speed would imply a slight reduction of the voltage available to produce torque, due to the need of a voltage margin to inject the HF signal. Fig. 6 shows the signal processing required for torque estimation. Inputs to the torque estimation block are the output voltage of the HF resonant current controllers v^{r*}_{sdqHF1}

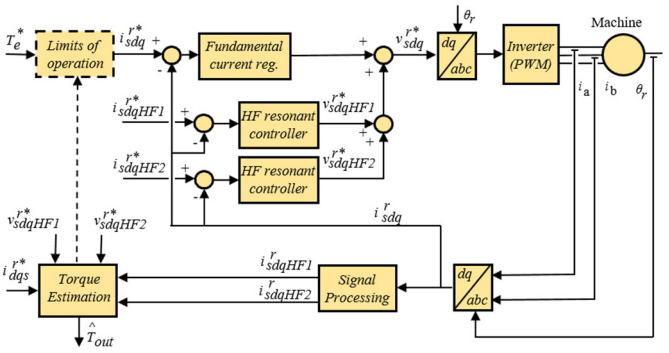

Fig. 5.- Injection of pulsating HF currents. Dashed lines indicate optional functionalities.

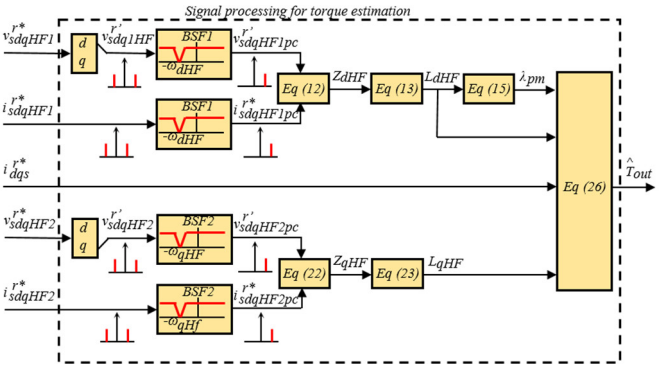

Fig. 6.- Schematic representation of the signal processing for torque estimation using pulsating HF current injection.

TABLE I. EXPERIMENTAL TESTS CONDITIONS				
I_{HF} [pu]	ω_{dHF} [rad/s]	ω_{qHF} [rad/s]	bw_{BSF1} [rad/s]	bw_{BSF2} [rad/s]
0.05	$2\cdot\pi\cdot500$	$2\cdot\pi\cdot1000$	$2\cdot\pi$ 10	$2\cdot\pi$ 10

TABLE II. MACHINE PARAMETERS				
P_{Rated} [kW]	V_{Rated} [V]	I_{Rated} [A]	ω_r [rpm]	Poles
4	350	14	1000	6

(9) and $v^{r'}_{sdqHF2}$ (19), the commanded HF currents i^{r*}_{sdqHF1} (7) and i^{r*}_{sdqHF2} (17) and the injected fundamental current i^{r*}_{sdq}, see Fig. 5. Two band stop filters, *BSF1* and *BSF2* are used to remove the negative sequence components of the HF currents and voltages. Implementation details are summarized in Table I. The d and q-axis HF impedances are estimated using (12) and (22), the d and q-axis HF inductances are estimated using (13) and (23), the PM flux is estimated using (15) and the output torque, T_{out}, is finally estimated using (26), by adding (16) and (25). Note that the proposed method does not require knowledge of PM temperature.

$$T_{out} = \frac{3}{2}\frac{P}{2}\left[\left(\lambda_{pm0} + k_{dPM}\frac{L_{dHF} - L_{dHF_0}}{L_{dHF_0}}\right) i^{r}_{sq} + \left(k_{f_{dHF}} L_{dHF} - k_{f_{qHF}} L_{qHF}\right) i^{r}_{sd} i^{r}_{sq}\right] \quad (26)$$

The proposed method has been tested in an IPMSM, driven by a power converter with 1200V, 100A IGBT power modules (7MBP100VDA120-50 [26]). The switching frequency is 10kHz, following a Standard Space Vector Modulation strategy. The machine used for experimental results is equipped with Grade 42-SH PMs. Fig. 7a shows the schematic representation of the machine used for the

verification of the method, the parameters being shown in Table II. The test machine was loaded with a commercial 40kW axial PMSM machines (EMRAX 228 [27]) driven by a *BAMOCAR-PG-D3* power converter [28]. Fig. 7b shows a picture of the test bench. Output torque of the test machine has been measured with an Interface Torque transducer [1] as shows Fig. 7b (T5 model, 12-Bit resolution, 10kHz, ±100Nm, 0.2% combined error). Test machine currents have been measured with standard 1% accuracy current transducers [29] and 12-bit analog-to-digital converters [30]. PMs temperatures were measured in real time using a wireless on-line measurement system [22], to assess the accuracy of the method.

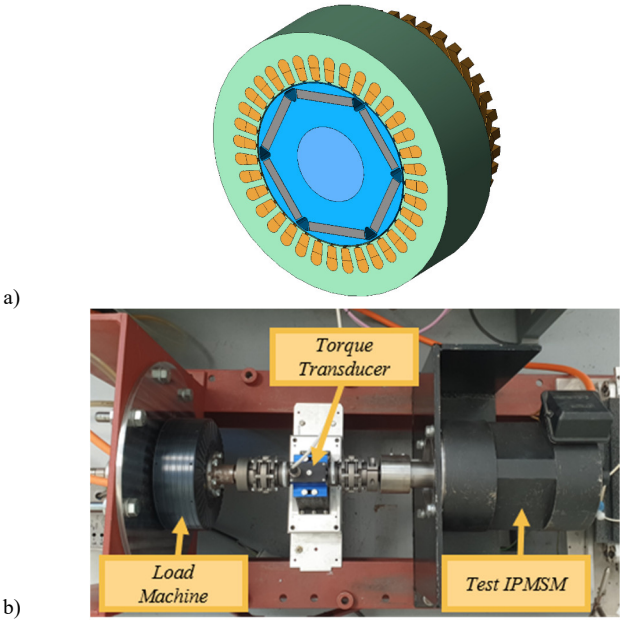

Fig. 7.- (a) Schematic representation of the test machine and (b) picture of the test bench.

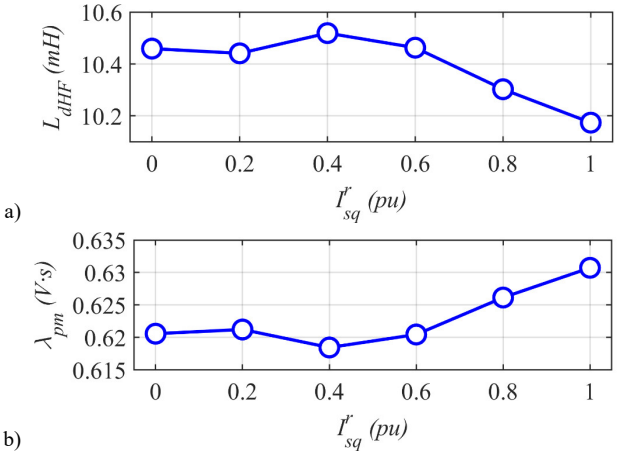

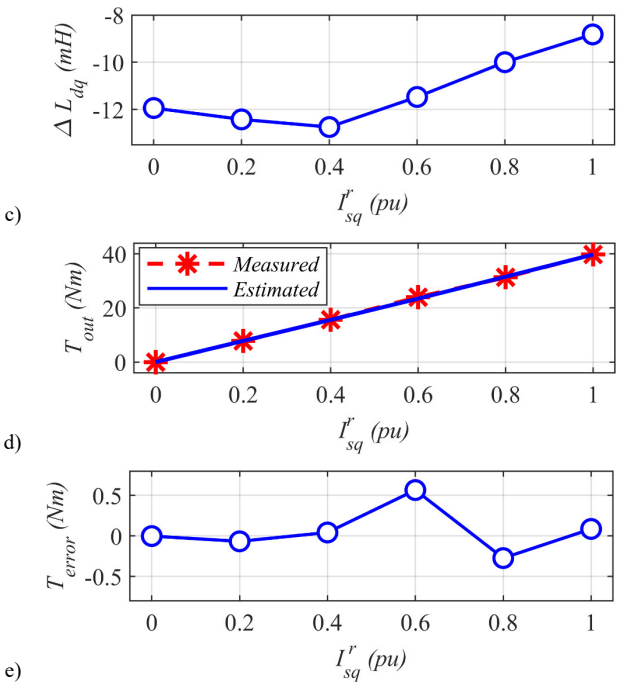

Fig. 8.- Experimental results: (a) Estimated *d*-axis HF inductance L_{dHF}, (b) Estimated PM flux, λ_{pm}; (c) Estimated differential inductance, i.e. $L_d - L_q$; (d) Estimated and measured torque; (e) Estimated torque error. $0 < I^r_{sq} < 1$pu, I^r_{sd}=0pu, I_{HF} = 0.05 pu, $\omega_{dHF} = 2\cdot\pi$ 500 rad/s and, $\omega_{qHF} = 2\cdot\pi$ 1000 rad/s, $\omega_1 = 2\cdot\pi$ 50 rad/s, $k_{fdHF} \approx 1.058$, $k_{fqHF} \approx 1.119$ and $k_{dPM} = -0.372$ Vs.

B) Experimental results

Fig. 8 shows experimental results when the magnitude of the *q*-axis component of the fundamental current, I^r_{sq}, changes from 0pu to 1pu. Fig. 8a shows the estimated *d*-axis HF inductance (13), L_{dHF}. Fig. 8b shows the estimated PM flux, λ_{pm}; L_{dHF} shown in Fig. 8a being used to estimate λ_{pm} (15). λ_{pm} is used to estimate the electromagnetic/synchronous torque (16). Fig. 8c shows the estimated differential inductance L_d-L_q, (24), obtained from the estimated *d*-axis HF inductance (13), and *q*-axis HF inductance L_{qHF}, (23). The reluctance

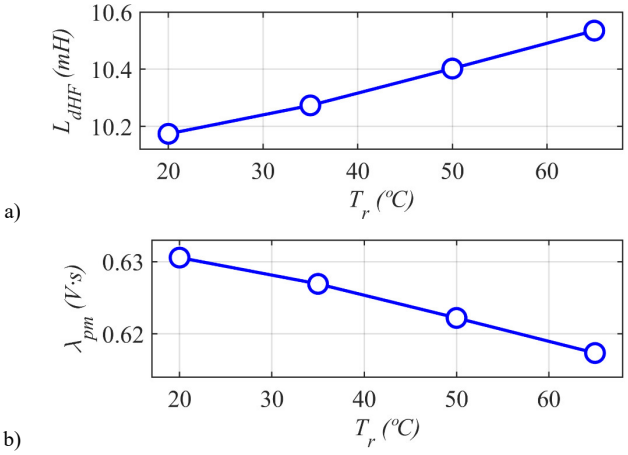

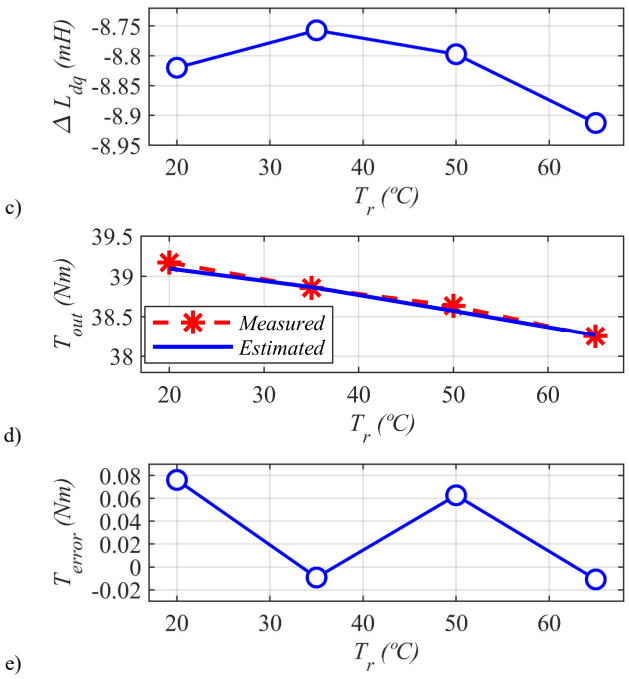

Fig. 9.- Experimental results: (a) Estimated d-axis HF inductance, L_{dHF}; (b) Estimated PM flux, λ_{pm}; (c) Estimated differential inductance, i.e. $L_d - L_q$; (d) Estimated and measured torque; (e) Estimated torque error. I^r_{sa} =1pu, I^r_{sd} =0pu, 20<Tr<65ºC, I_{HF} = 0.05 pu, $\omega_{dHF} = 2\cdot\pi$ 500 rad/s and, $\omega_{qHF} = 2\cdot\pi$ 1000 rad/s, $\omega_1 = 2\cdot\pi$ 50 rad/s, $k_{fdHF} \approx 1.058$, $k_{fqHF} \approx 1.119$ and $k_{dPM} = -0.372$ Vs.

torque (25) is estimated from the differential inductance. Fig. 8d shows the estimated, (26), and measured torque of the machine while Fig. 8e shows the error in the torque estimation. It is noted that the error is <0.5 Nm, which is within the tolerance band of the torque sensor of 0.2%. Another potential explanation for this error would be that the estimated torque is the electromagnetic torque, (26), while the measured torque is the shaft torque (see Fig. 7), which is affected by windage and friction losses. However, the fact that the sign of the error in Fig. 8e varies for the different operating points makes this explanation arguable.

Fig. 9 shows analogous results to Fig. 8 but when I^r_{sa} = 1pu (I^r_{sd} = 0) and PM temperature changes from 20ºC to 65ºC. An increase of the PM temperature results in a reduction of PM flux, λ_{pm}, and consequently of the output torque. It is observed from Fig. 9e that the error in the estimated torque in this case is <0.1 Nm.

Fig. 10 shows the performance of the proposed method in the whole I^r_{sa} - I^r_{sd} map. Fig. 10a-c shows measured and estimated torques and the estimation error respectively. Current circle limit, i.e. $|i^r_{sda}| = I^r_{sda} = 1$ pu, as well as Maximum Torque per Ampere (MTPA) trajectory (OA), constant power region (1st flux weakening region, AB) and Maximum Torque per Volt (MTPV) trajectory (2nd flux weakening region, BC) are also indicated in the figure. It can be seen from Fig. 10c that q-axis current has almost no impact on the torque estimation error, larger errors occurring in the deep flux-weakening region, 0< I^r_{sq} <0.1 pu and -1< I^r_{sd} <-0.9 pu; the maximum error being <6Nm. It must be noted however that this region does not belong to the trajectory OABC which would be followed normally. Errors in the estimated torque along the OABC trajectory are shown in Fig. 11. Fig. 11a-c shows the estimated torque error when the fundamental dq-axis current, I^r_{sda}, changes from 0 to 1pu following the MTPA trajectory (OA), when the fundamental dq-axis current, I^r_{sda} follows the constant power region trajectory (AB) and I^r_{sda} following the MTPV trajectory (BC), respectively. The maximum estimated error is seen to be <2.5Nm.

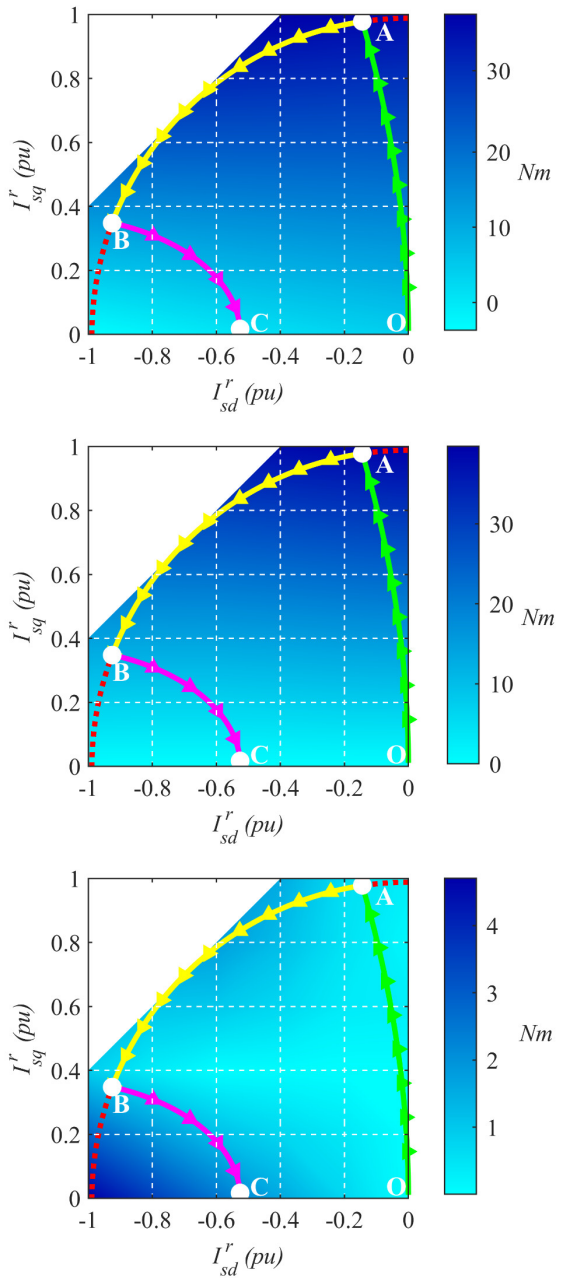

Fig. 10.- Experimental results: (a) Measured torque vs I^r_{sa} and I^r_{sd}; (b) Estimated torque; (c) Estimated torque error. 0< I^r_{sa} <1pu, -1< I^r_{sd} <0pu, T_r =20ºC, I_{HF} = 0.05 pu, $\omega_{dHF} = 2\cdot\pi$ 500 rad/s and, $\omega_{qHF} = 2\cdot\pi$ 1000 rad/s, $\omega_1 = 2\cdot\pi$ 50 rad/s, $k_{fdHF} \approx 1.058$, $k_{fqHF} \approx 1.119$ and $k_{dPM} = -0.372$ Vs.

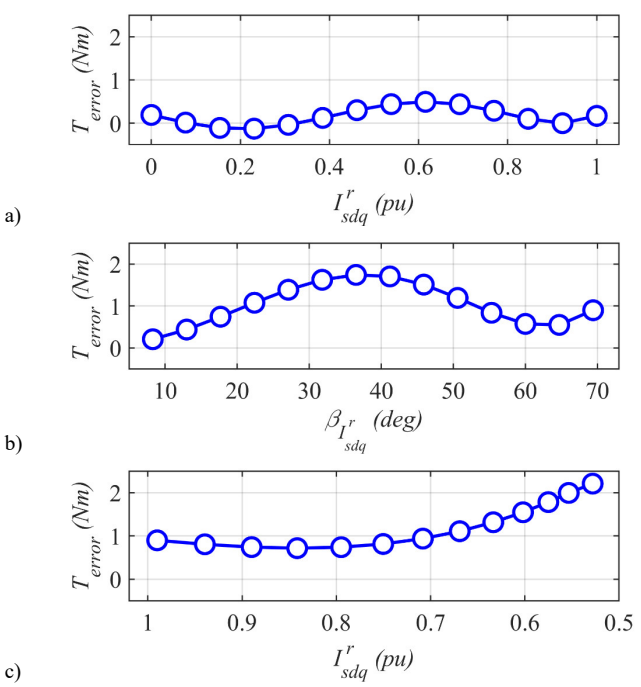

Fig. 11.- Experimental results. Estimated torque error: (a) MTPA trajectory (OA); (b) constant current trajectory (AB); (c) MTPV trajectory (BC), T_r =20ºC, I_{HF} = 0.05 pu, $\omega_{dHF} = 2{\cdot}\pi$ 500 rad/s and, $\omega_{qHF} = 2{\cdot}\pi$ 1000 rad/s, $\omega_1 = 2{\cdot}\pi$ 50 rad/s, $k_{fdHF} \approx 1.058$, $k_{fqHF} \approx 1.119$ and $k_{dPM} = -0.372$ Vs.

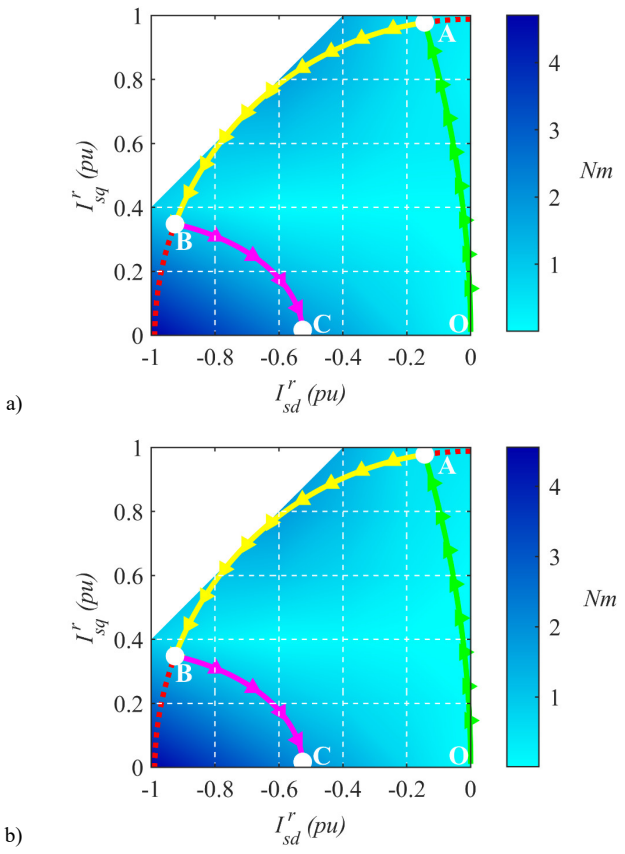

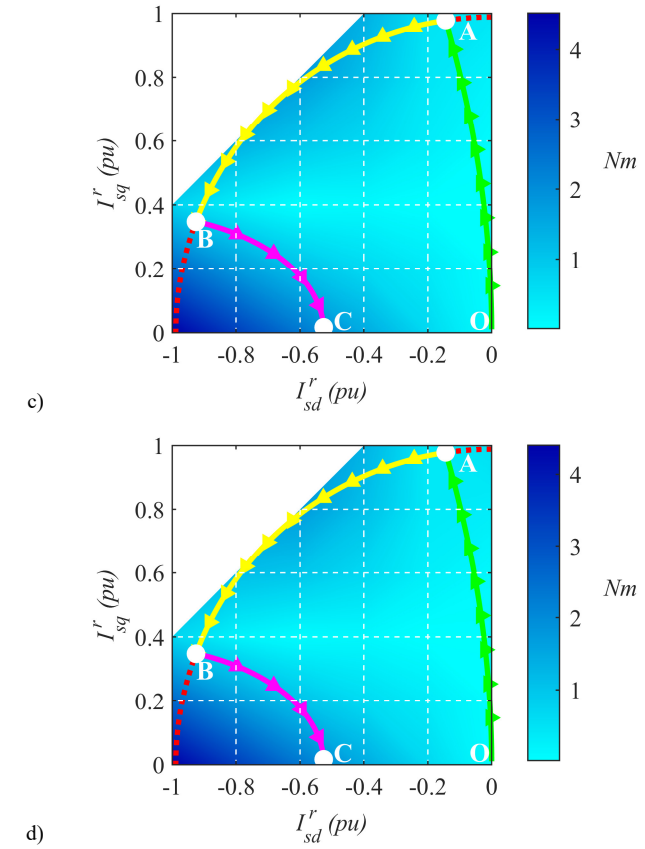

Fig. 12.- Experimental results: Estimated torque error at (a) T_r =20ºC; (b) T_r =35ºC; (c) T_r =50ºC; (d) T_r =65ºC. $0 < I^r_{sq} < 1$ pu, $-1 < I^r_{sd} < 0$ pu, I_{HF} = 0.05 pu, $\omega_{dHF} = 2{\cdot}\pi$ 500 rad/s and, $\omega_{qHF} = 2{\cdot}\pi$ 1000 rad/s, $\omega_1 = 2{\cdot}\pi$ 50 rad/s, $k_{fdHF} \approx 1.058$, $k_{fqHF} \approx 1.119$ and $k_{dPM} = -0.372$ Vs.

Fig. 13.- Experimental results: Estimated torque error at T_r =20ºC; 35ºC; 50ºC and 65ºC: (a) MTPA trajectory (OA); constant current trajectory (AB); (c) MTPV trajectory (BC). I_{HF} = 0.05 pu, $\omega_{dHF} = 2{\cdot}\pi$ 500 rad/s and, ω_{qHF} =

$2 \cdot \pi$ 1000 rad/s, $\omega_1 = 2 \cdot \pi$ 50 rad/s, $k_{fdHF} \approx 1.058$, $k_{fqHF} \approx 1.119$ and $k_{dPM} = -0.372$ Vs.

Finally, Fig. 12a-d shows the torque estimation error for four different PMs temperatures of 20, 35, 50 and 65ºC. The estimated error when the fundamental *dq*-axis current moves along the OABC trajectory being shown in Fig. 13. It can be observed from both figures that torque estimation error is barely affected by PM temperature variation.

V. Conclusions

This paper proposes permanent magnet synchronous machines online torque estimation based on the torque equation combined with parameter identification. The proposed method uses a modified torque equation, which relies on the high frequency *d* and *q*-axes inductances of the machine. The inductances are estimated from the response to two high frequency signals, which are superposed on top of the fundamental excitation applied by the inverter. The proposed method operates therefore without interfering with the normal operation of the machine. Extensive experimental results under different operating conditions have been provided to demonstrate de viability of the proposed method.

VI. References

[1] http://www.interfacetorque.co.uk
[2] https://www.hbm.com
[3] http://www.futek.com
[4] http://www.magtrol.com/torque
[5] http://www.te.com
[6] G. Heins, M. Thiele and T. Brown, "Accurate Torque Ripple Measurement for PMSM." IEEE Trans. on Instrumentation and Measurement, 60(12): 3868-3874, Dec. 2011.
[7] P. Sue, D. Wilson, L. Farr and A. Kretschmar, "High precision torque measurement on a rotating load coupling for power generation operations," IEEE International Instrumentation and Measurement Technology Conference Proceedings, pp. 518-523, May 2012.
[8] K. C. Yeo, G. Heins and F. De Boer, "Comparison of torque estimators for PMSM," AUPEC, pp. 1-6, Dec. 2008.
[9] B. Cheng and T. R. Tesch, "Torque Feedforward Control Technique for Permanent-Magnet Synchronous Motors", IEEE Trans. on Ind.Electr., 57(3): 969-974, March 2010.
[10] F. Jukic, D. Sumina and I. Erceg, "Comparison of Torque Estimation Methods for Interior Permanent Magnet Wind Power Generator", IEEE EDPE, pp. 291-296, Oct 2017.
[11] Weizhe Qian, S.K. Panda, and Jian-Xin Xu, "Improved PMSM pulsating torque minimization with iterative learning and sliding mode observer", IECON, pp. 1931-1936, Oct 2000.
[12] B. H. Lam, S. K. Panda, J. x. Xu and K.W. Lim 'Torque ripple minimization in PM synchronous motor using iterative learning control', IEEE PED, pp. 141-149, July 1999.
[13] S. -K. Chung, H. -S. Kim, C. -G. Kim and M. -J. Youn, 'A new instantaneous torque control of PM synchronous motor for high-performance direct drive applications', IEEE Trans. Power Elect., 13(3): 388-400, May 1998.
[14] Xu Dong and Wang Tianmiao and Wei Hongxing, "Comparison between model reference observer and reduced order observer of PMSM torque", IEEE-ICIEA, pp. 663-667, June 2011.
[15] Q. Liu and K. Hameyer ,"High-Performance Adaptive Torque Control for an IPMSM With Real-Time MTPA Operation ", IEEE Trans. on Energy Conv., 32(2): 571-581, June 2017.
[16] Y.-R. Mohamed and T. K. Lee, "Adaptive self-tuning MTPA vector controller for IPMSM drive system," IEEE Trans. Energy Conv., 21(3): 636–644, Sep. 2006.
[17] W. F. Traoré and R. McCann, "Torque measurements in synchronous generators using giant magnetoresistive sensor arrays via the Maxwell stress tensor," IEEE Power & Energy Society General Meeting, pp. 1-5, Jul 2013.
[18] Z. Lin, D. S. Reay, B. W. Williams, and X. He, "Online modeling for switched reluctance motors using B-spline neural networks," IEEE Trans. Ind. Electron., 54(6): 3317-3322, Dec. 2007.
[19] J. F. Gieras and M. Wing, "Permanent magnet motor technology: design and application". Second edition 2002.
[20] N. Limsuwan, T. Kato, K. Akatsu, and R. D. Lorenz, "Design and evaluation of a variable-flux flux-intensifying interior permanent-magnet machine," IEEE Trans. Ind. Appl., 50(2): 1015–1024, Mar./Apr. 2014.
[21] H. Jung, D. Park, H. Kim, S. Sul and D. J. Berry, "Non-Invasive Magnet Temperature Estimation of IPMSM Based on High-Frequency Inductance With a Pulsating High-Frequency Voltage Signal Injection," IEEE Trans. Ind. Appl., 55 (3): 3076-3086, May-June 2019.
[22] D. Reigosa, D. Fernández, M. Martínez, J. M. Guerrero, A. B. Diez and F. Briz, "Magnet Temperature Estimation in Permanent Magnet Synchronous Machines Using the High Frequency Inductance," IEEE Trans. Ind. Appl., 55(3): 2750-2757, May-June 2019.
[23] M. Martinez, D. Reigosa, D. Fernandez, J.M. Guerrero and F. Briz, "PMSMs Torque Estimation Using Pulsating HF Current Injection", IEEE-SLED, pp. 96-101, Sept. 2018.
[24] D. Reigosa, D. Fernandez, H. Yoshida, T. Kato and F. Briz "Permanent-Magnet Temperature Estimation in PMSMs Using Pulsating High-Frequency Current Injection," IEEE Trans. on Ind. Appl., 51(4): 3159–3168, July-Aug 2015.
[25] Fukushige, N. Limsuwan, T. Kato, K. Akatsu, and R. D. Lorenz, "Efficiency contours and loss minimization over a driving cycle of a variable flux-intensifying machine," IEEE Trans. Ind. Appl., 51(4): 2984–2989, Jul./Aug. 2015
[26] https://www.fujielectric.com/products/semiconductor/model/igbt
[27] https://emrax.com
[28] https://www.unitek-industrie-elektronik.de
[29] https://www.lem.com/sites/default/files/products_datasheets/la_25-p.pdf
[30] http://www.ti.com/product/TMS320F28335#